ANALYSIS OF ROCK POWDERS BY LASER-INDUCED BREAKDOWN SPECTROSCOPY COMBINED WITH THE GRAPHITE DOPING METHOD**

J. J. Jia [1,2], F. Hongbo [1], W. Huadong [1,2], D. Fengzhong [1,2], Z. Zhirong [1,2*]

[1] Anhui Provincial Key Laboratory of Photonic Devices and Materials, Anhui Institute of Optics and Fine Mechanics, Chinese Academy of Science, Hefei 230031, China; e-mail: jjw2014@mail.ustc.edu.cn
[2] University of Science and Technology of China, Hefei 230026, China

The analysis of geological samples using laser-induced breakdown spectroscopy (LIBS) is strongly affected by matrix effects. To investigate the improvement of matrix effects by the graphite doping method, rock powder was mixed with graphite powder and pressed into pellets. Four groups of samples with the same graphite content were prepared from a mixture of seven different rock powders and four graphite powders (0, 25, 50, and 75 wt.%). To reduce some of the pulse-to-pulse fluctuations, the internal standardization method was adopted. Four sets of calibration curves of Ca and Mg were prepared using pellet samples with the same graphite content. The influence of graphite content on laser-induced plasma temperature and electron density was further investigated. The coefficients of determination (R^2) of the calibration curves after doping graphite are larger than those without doping, and the stability of the spectral intensity, plasma temperature, and electron density after doping are also improved. In particular, when the doping percentage is 50%, the matrix effect is significantly improved. The results show that the graphite doping method has great potential for improving the matrix effects of LIBS in the analysis of rock powder samples.

Keywords: *laser-induced breakdown spectroscopy, matrix effects, grafite doping, rock powder.*

АНАЛИЗ ПОРОШКОВ ГОРНЫХ ПОРОД МЕТОДОМ ЛАЗЕРНО-ИНДУЦИРОВАННОЙ ИСКРОВОЙ СПЕКТРОСКОПИИ В СОЧЕТАНИИ С МЕТОДОМ ЛЕГИРОВАНИЯ ГРАФИТОМ

J. J. Jia [1,2], F. Hongbo [1], W. Huadong [1,2], D. Fengzhong [1,2], Z. Zhirong [1,2*]

УДК 533.9;546.26-162

[1] Главная лаборатория фотонных приборов и материалов провинции Аньхой, Аньхойский институт оптики и точной механики Китайской академии наук, Хэфэй 230031, Китай; e-mail: jjw2014@mail.ustc.edu.cn
[2] Университет науки и технологии Китая, Хэфэй 230026, Китай

(Поступила 29 июня 2019)

Исследована возможность подавления матричных эффектов путем добавки графита при анализе геологических образцов методом спектроскопии лазерно-индуцированной плазмы (LIBS). С этой целью образцы порошков горной породы смешивались с графитовым порошком с последующим прессованием в таблетки. Четыре группы образцов с одинаковым содержанием графита приготовлены из смеси семи различных порошков горной породы и четырех графитовых порошков (0, 25, 50 и 75 мас.%). Для уменьшения влияния флуктуаций от импульса к импульсу использован метод внутренней стандартизации. С использованием образцов таблеток с одинаковым содержанием графита получены четыре набора калибровочных кривых для Ca и Mg. Исследовано влияние содержания графита на температуру и электронную плотность лазерно-индуцированной плазмы. Коэффициенты

** Full text is published in JAS V. 87, No. 5 (http://springer.com/journal/10812) and in electronic version of ZhPS V. 87, No. 5 (http://www.elibrary.ru/title_about.asp?id=7318; sales@elibrary.ru).

детерминации (R^2) калибровочных кривых после легирования графитом оказались больше, чем без легирования, стабильность спектральной интенсивности, температуры и электронной плотности плазмы после легирования также улучшилась. Влияние матричного эффекта значительно снижается, когда легирование достигает 50%. Показано, что метод легирования графитом имеет большой потенциал для снижения влияния матричных эффектов при анализе образцов порошка горных пород методом спектроскопии лазерно-индуцированной плазмы.

Ключевые слова: *спектроскопия лазерно-индуцированной плазмы, матричные эффекты, легирование графитом, порошок горных пород.*

Introduction. The chemical composition of rocks is of great value in the exploration of petroleum, natural gas, and mineral resources. Common analytical techniques used for the elemental analysis of rocks or minerals include scanning electron microscope-energy dispersive spectrometry (SEM-EDS) [1], X-ray fluorescence (XRF) [2], micro-computed tomography (CT) [3], and laser ablation inductively coupled plasma mass spectrometry (LA-ICP-MS) [4]. However, these techniques have inherent limitations [5]. Laser-induced breakdown spectroscopy (LIBS) is a type of the atomic emission spectroscopic technique for elemental detection of solid, liquid, gas, or aerosol samples [6]. In the last decade, LIBS has drawn much attention for its advantages of rapid multi-element analysis, nondestructivity, and remote online analysis with minimal sample pre-treatment. Due to its unique advantages, LIBS has been successfully applied in space exploration [7], quality monitoring [8, 9], environmental monitoring [10, 11], and other fields [12–14].

Due to severe matrix effects, it is difficult to quantitatively analyze geological samples with complex matrices by LIBS. Since rock is a natural target with various and complex matrices, it is still impractical to prepare matrix-matched standards for practical applications. To overcome the challenge, diverse approaches, such as microwave-enhanced [15], spark discharge-assisted [16], and data processing methods [17, 18], have been proposed. Although these methods achieved some progress in improving the matrix effects, the advantages of LIBS will be limited due to time-consuming data processing, complex sample preparation, or increased cost and complexity of the system.

When analyzing powder samples using LIBS, some auxiliary materials, such as KBr [19], H_3BO_3 [20], or PVA [21], need to be added into the powder samples to prepare pellets. However, these materials are only used as a binder, making the powder sample easy to shape, and the amount of the addition is rarely considered. Moreover, the sample to be analyzed must not contain the components in the binder, otherwise, the accuracy of the analysis results will be seriously affected.

Graphite powder is widely used in the fields of casting, batteries, carbon products, and refractories because of its chemical stability, simple composition, high-temperature resistance, and good lubricity and plasticity. In this work, Ca and Mg elements in three types of rock samples (volcanic rocks, limonite sedimentary rocks, and metamorphic rocks) with different matrices were analyzed using LIBS combined with the graphite doping method. The aim of this work is to study the improvement of matrix effects by graphite doping methods.

Experimental. As presented in Fig. 1, a *Q*-switched Nd: YAG laser (DAWA, Beamtech) operating at the wavelength of 1064 nm with 1 Hz repetition rate and 7 ns pulse duration was used as the excitation source to generate the plasma. The fixed energy of a 35 mJ laser beam was focused onto the sample surface with a mirror (beam splitter 1) and an UV-grade quartz double-convex lens (focusing lens 1) with a focal length of 100 mm. The plasma emission spectrum was coupled into a 1.5 m long quartz fiber by a mirror (beam splitter 2) and a collecting lens with a focal length of 25 mm. The spectrometer used throughout the experiment was an Echelle spectrometer with an intensified CCD detector (Andor, Mechelle 5000) with a resolution of $\lambda/\Delta\lambda \geq 5{,}000$ in the 220 and 950 nm spectral region. The spectrometer was connected to a PC for data storage and spectrum analysis. The values of 3.0 μs and 550 ns were used as the delay time and the gate width, respectively. To provide a fresh position and avoid deep craters, the sample was mounted on an auto-controlled XYZ motorized stage. Each sample was analyzed using 10 locations with 20 shots averaged together, resulting in 10 spectra per sample. To minimize any surface contamination, the first five shots were discarded. The camera above the system is primarily used to view and image the surface of the sample.

Three volcanic rock (granite, andesite, and basalt, 01#-03#), one limonite sedimentary rock (shale, 04#), two metamorphic rock (gneiss and amphibolite, 05#-06#) certified powder samples (Institute of Geophysical and Geochemical Exploration, Chinese Academy of Geological Sciences), and a graphite powder sample (purity of 99.99%) were employed in this work. Table 1 lists the certified elemental concentrations of Ca, Mg, and Si elements in the samples. The rock powder sample was individually mixed with graphite powder

at percentages of 0, 25, 50, and 75%. The mixture was homogenized and ground in an agate mortar and pressed into 20 mm diameter and 3 mm thickness pellets with an electric hydraulic jack under a pressure of 25 MPa.

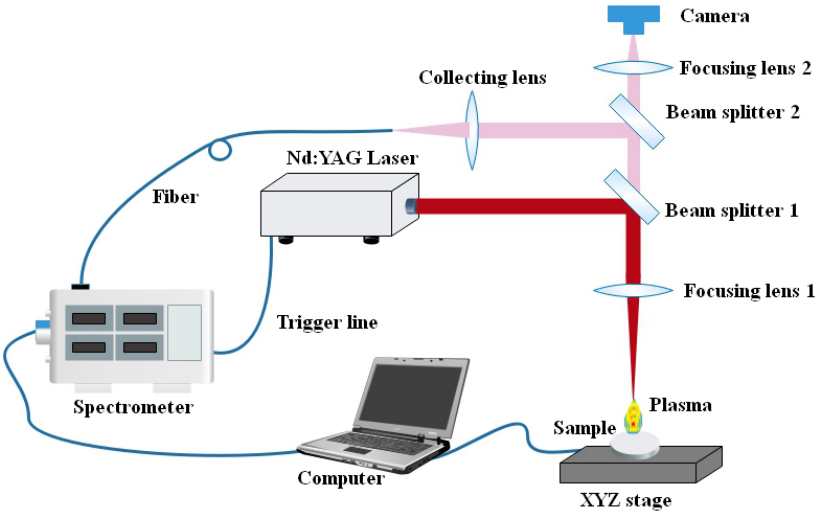

Fig. 1. Schematic diagram of the experimental setup.

TABLE 1. Certified Elemental Concentrations in the Samples (wt.%)

Sample No.	01#	02#	03#	04#	05#	06#
Ca	1.55	5.20	8.81	0.60	2.66	9.60
Mg	0.42	1.72	7.77	2.01	1.63	7.20
Si	72.83	60.62	44.64	59.23	66.27	49.62

Results and discussion. *Calibration curves for Ca and Mg.* Figure 2 shows a characteristic spectrum from sample 02# doped with different percentages of graphite powder. As the graphite content increases, the concentration of elements in the rock decreases, resulting in a decrease in the spectral intensity. Several lines of Mg (Mg II 279.55 nm, Mg II 280.27 nm, Mg I 285.21 nm), Si (Si I 288.16 nm), and Ca (Ca II 315.89 nm, Ca II 317.93 nm) were identified in the spectrum based on the National Institute of Standards and Technology (NIST) database. The spectral lines of Ca I 315.9 nm and Mg II 285.21 nm were selected as the analysis lines to avoid interference from other lines.

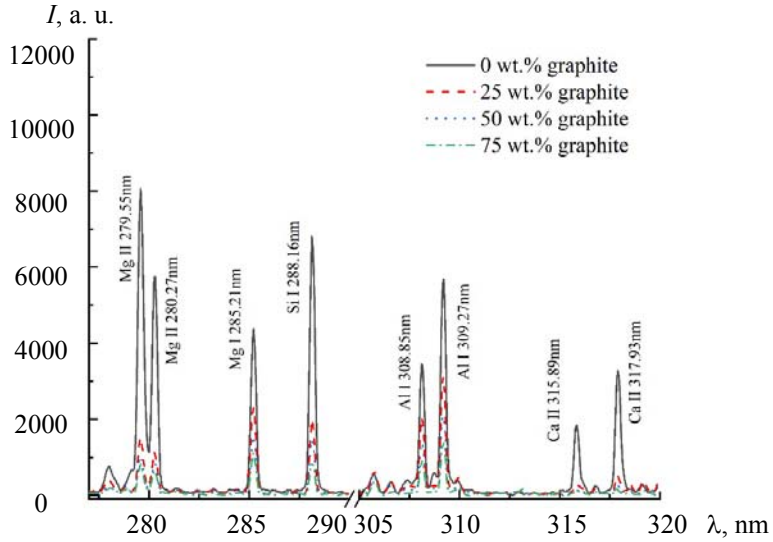

Fig. 2. Spectral lines from 02# sample with different percentages of graphite.

To reduce some of the pulse-to-pulse fluctuations, the internal standardization method was adopted. The spectral line of each element was normalized to the major element Si II 288.16 nm line, as presented:

$$I^i_{\text{element}} = S^i_{\text{element}} / S^i_{\text{Si}},\ i = 1,2,...,n, \quad (1)$$

where I, S_{element}, and S_{Si} are the intensity of the analysis line and the integration area under the lines of the element i and Si, respectively.

The calibration curves for Ca and Mg elements with different percentages of graphite are present in Fig. 3. The x-axis and y-axis refer to elemental concentrations and normalized spectral intensities of Ca and Mg elements, respectively. The determination coefficient (R^2) of the calibration curves and the error bars were used to evaluate the performance of the calibration models. The error bars corresponded to the standard deviation (SD) of the spectral intensities from 10 replicate measurements.

The smaller the SD value, the more stable the measurement. The larger the R^2 value, the better the linearity of the spectral intensity and concentration, and the more accurate the prediction result. The SD values of the spectral intensity of the doped graphite samples became smaller, indicating that after doped graphite the spectral stability was improved. As shown in Fig. 3a, the R^2 value of Ca curve increased from 0.913 to 0.960, 0.992, and 0.925. The R^2 value for the Mg curve also increased from 0.905 to 0.932, 0.969, and 0.917, as shown in Fig. 3b. It can be concluded that the matrix effect of the analysis of the rock powder samples was improved by doping graphite. In particular, when the doping percentage is 50%, the R^2 values of both the Ca and Mg calibration curves were the largest, and the SD of the intensity was also the smallest.

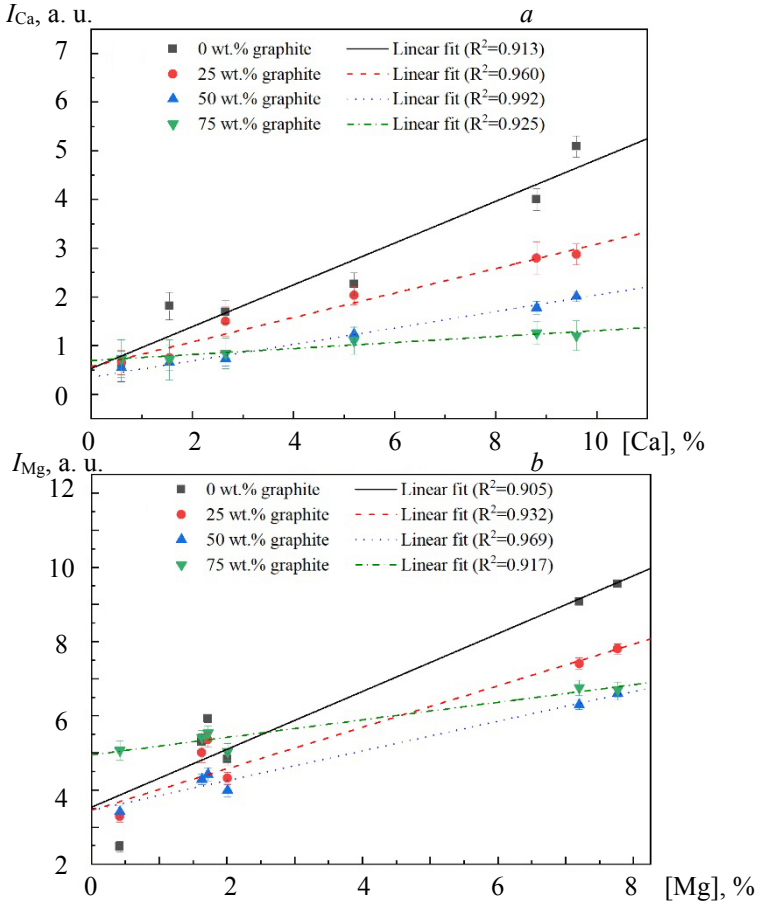

Fig. 3. Calibration curves of elements (a) Ca and (b) Mg with different percentages of graphite.

Effect on the plasma temperature and electron density. The intensity of an emission spectra line can be calculated by

$$I_k = FC_s \frac{g_k A_{ki}}{U(T)} \exp \frac{E_k}{k_B T}, \quad (2)$$

where I_k is the line intensity, A_{ki} is the transition probability, E_k is the high energy level transition energy,

g_k is the upper-level degeneracy, k_B is the Boltzmann constant, F is the experimentally related constant, T is the plasma temperature, and $U(T)$ is the partition function. The parameters of g_k, A_{ki}, and E_k can be obtained from the NIST database.

According to Eq. (2), since the intensity is mainly determined by the plasma temperature, it is necessary to study the stability of the plasma temperature. In this work, the plasma temperature was measured using the Boltzmann plot method [22]. Here, five Ca atomic lines were selected for preparing the Boltzmann plot, and the parameters of the lines are listed in Table 2.

TABLE 2. Parameters of Ca Atomic Lines Used to Calculate Plasma Temperature

Wavelength, nm	A_{ki} ($10^8 s^{-1}$)	g_k	E_i, eV	E_k, eV
443.6	0.342	3	4.6801799	4.6801799
610.3	0.096	3	3.9103990	3.9103990
612.2	0.287	3	3.9103990	3.9103990
643.9	0.530	9	4.4506470	4.4506470
646.3	0.470	7	4.4409544	4.4409544

In addition to the plasma temperature, the electron density is also an important parameter for plasma. According to the laser-plasma broadening theory, the line broadening mainly occurs due to the Stark broadening caused by the collision of particles in the plasma, and from the relationship shown in Eq. (3), the electron density N_e can be measured:

$$\Delta\lambda_{FWHM} = 2\times10^{-16}\omega N_e, \quad (3)$$

where ω is the electron impact width parameter obtained from the literature [23], $\Delta\lambda_{FWHM}$ is the full width at half maximum of the Stark broadening lines, and N_e is the electron density. In this paper, the electron density was calculated by the Stark broadening of an atomic line of Ca at 422.7 nm.

As shown in Fig. 4, the plasma temperature of sample 02# with different graphite contents estimated by the Boltzmann plot method was 8116, 7832, 7645, and 7491 K. The electron density estimated by Eq. (2) was 4.67×10^{16}, 4.46×10^{16}, 4.18×10^{16}, and 3.81×10^{16} cm^{-3}.

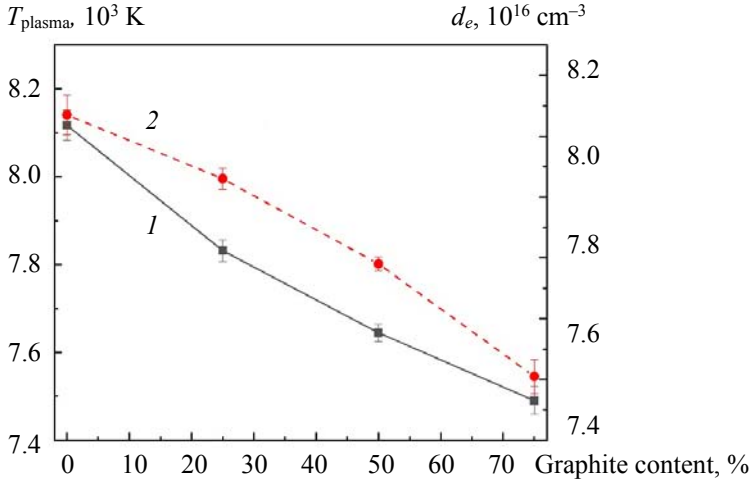

Fig. 4. Change of plasma temperature (1) and electron density (2) of 02# sample with different graphite contents.

The McWhirter criterion [24] was described by Eq. (4), which must be met by the plasma to be in local thermodynamic equilibrium (LTE), in which the excited state particles follow the Boltzmann distribution.

$$N_e \geq 1.6\times10^{12}T^{1/2}\Delta E^3, \quad (4)$$

where T and ΔE (eV) denotes the plasma temperature and the largest transition energy between the states (2.93 eV for Ca I 422.7 nm), respectively. At 8116, 7832, 7645, and 7491 K, N_e of the samples with different amounts of graphite doping are 3.63×10^{15}, 3.56×10^{15}, 3.52×10^{15}, and $3.48\times10^{15}$$cm^{-3}$, which is lower than the electron density determined in the experiments. The plasma produced from the samples of different graphite

doping amounts satisfies the LTE state.

Although the plasma temperature and electron density decreased due to decrease in the elemental concentration in the samples, the SD values also decreased, especially for the samples with a graphite doping amount of 50%. The more stable the plasma temperature and electron density, the more stable the generated plasma, which will also make the spectral intensity more stable. It also proved that the use of the doping graphite method could effectively improve the matrix effect of LIBS analysis.

Conclusions. The influence of the graphite doping method on the improvement of matrix effects of LIBS for the analysis of rock powdered samples was investigated in detail. The analytical performance was evaluated by comparing R^2 values of the calibration curves and SD values of the spectral intensity. After doping graphite, the R^2 values are larger than those without doping, and the stability of the spectral intensity, plasma temperature, and electron density after doping are also improved. In particular, when the graphite doping percentage is 50%, the matrix effect is significantly improved. The plasma produced from samples of different graphite doping content all satisfies the LTE state. The results show that the doped graphite method can effectively improve the matrix effect when using LIBS to analyze rock powder samples.

Acknowledgments. This research was supported by the National Natural Science Foundation of China (Grant N 61505223), and the project of China State Key Laboratory of Power Systems (Grant N SKLD18KM11).

REFERENCES

1. G. Poupeau, F. X. L. Bourdonnec, T. Carter, S. Delerue, M. S. Shackley, J. A. Barrat, S. Dubernet, P. Moretto, T. Calligaro, M. Milić, K. Kobayashi, *J. Archaeol. Sci.*, **37**, N 11, 2705–2720 (2010).
2. T. D. T. Oyedotun, *Geol., Ecol., Landscapes*, **2**, N 2, 148–154 (2018).
3. X. Chen, G. Yao, J. Cai, Y. Huang, X. Yuan, *J. Nat. Gas Sci. Eng*., **48**, 145–156 (2017).
4. J. M. Scott, J. M. Palin, *N. Z. J. Geol. Geophys.*, **51**, N 2, 105–113 (2008).
5. A. K. Rai, G. S. Maurya, R. Kumar, A. K. Pathak, J. K. Pati, Aw. K. Rai, *J. Appl. Spectrosc.*, **83**, N 6, 1089–1095 (2017).
6. D. A. Cremers, L. J. Radziemski, *Handbook of Laser-Induced Breakdown Spectroscopy*, Cambridge University Press, New York, 110–111 (2006).
7. A. Koujelev, V. Mottoros, D. Gratton, A. Dudelzak, *Can. Aeronaut. Space J.*, **55**, N 2, 97–106 (2009).
8. F. C. Alvira, G. M. Bilmes, T. Flores, L. Ponce, *Appl. Spectrosc.*, **69**, N 10, 1205–1209 (2015).
9. S. Awasthi, R. Kumar, A. K. Rai, *J. Appl. Spectrosc.*, **84**, 1–5 (2017).
10. S. S. Golik, O. A. Bukin, A. A. Il'in, E. B. Sokolova, A. V. Kolesnikov, M. Yu. Babiy, Yu. N. Kul'chin, A. A. Gal'chenko, *J. Appl. Spectrosc.*, **79**, N 3, 471–476 (2012).
11. S. Pandhija, N. K. Rai, A. K. Rai, S. N. Thakur, *Appl. Phys. B: Lasers Opt.*, **98**, N 1, 231–241 (2010).
12. S. A. Beldjilali, E. Axente, A. Belasri, T. Baba-Hamed, *J. Appl. Spectrosc.*, **84**, N 3, 472–477 (2017).
13. M. Dell'Aglio, R. Gaudiuso, G. S. Senesi, A. D. Giacomo, C. Zaccone, M. T. Miano, O. D. Pascale, *J. Environ. Monit.*, **13**, N 5, 1422–1426 (2011).
14. P. Singh, E. Mal, A. Khare, S. Sharma, *J. Cult. Herit.*, **33**, 71–82 (2018).
15. M. Wall, Z. Sun, Z. T. Alwahabi, *Opt. Express*, **24**, N 2, 1507 (2016).
16. Z. Hou, Z. Wang, J. Liu, W. Ni, Z. Li, *Opt. Express*, **22**, N 11, 12909 (2014).
17. M. Singh, V. Karki, A. Sarkar, *J. Appl. Spectrosc.*, **83**, N 3, 497–503 (2016).
18. D. Andrade, M. Sperança, E. R. Pereirafilho, *Anal. Methods*, **9**, N 35, 5156 (2017).
19. R. J. Lasheras, J. Anzano, C. Bellogálvez, M. Escudero, J. O. Caceres, *Anal. Lett.*, **50**, N 8, 1325–1334 (2016).
20. Z. Zhu, J. Li, Y. Guo, X. Cheng, Y. Tang, L. Guo, X. Li, Y. Lu, *J. Anal. At. Spectrom.*, **33**, N 2, 205 (2017).
21. A. A. I. Khalil, M. A. Morsy, H. Z. Eldeen, *Opt. Laser Technol.*, **96**, 227–237 (2017).
22. S. Pandhija, N. K. Rai, A. K. Rai, S. N. Thakur, *Appl. Phys. B: Lasers Opt.*, **98**, N 1, 231–241 (2010).
23. H. Griem, *Plasma Spectroscopy*, McGraw-Hill, New York, 320–357 (1964).
24. T. Fujimoto, R. W. Mcwhirter, *Phys. Rev. A*, **42**, N 11, 6588–6591 (1990).